

Document downloaded from:

<http://hdl.handle.net/10251/154118>

This paper must be cited as:

Cored-Bandrés, J.; Garcia-Ortiz, A.; Iborra Chornet, S.; Climent Olmedo, MJ.; Liu, L.; Chuang, C.; Chan, T.... (2019). Hydrothermal Synthesis of Ruthenium Nanoparticles with a Metallic Core and a Ruthenium Carbide Shell for Low-Temperature Activation of CO<sub>2</sub> to Methane. *Journal of the American Chemical Society*. 141(49):19304-19311.  
<https://doi.org/10.1021/jacs.9b07088>



The final publication is available at

<https://doi.org/10.1021/jacs.9b07088>

Copyright American Chemical Society

Additional Information

## **Hydrothermal synthesis of ruthenium nanoparticles with a metallic core and a ruthenium carbide shell for low temperature activation of CO<sub>2</sub> to methane**

Jorge Cored<sup>a</sup>, Andrea García-Ortiz<sup>a</sup>, Sara Iborra<sup>a</sup>, María J. Climent<sup>a</sup>, Lichen Liu<sup>a</sup>, Cheng-Hao Chuang<sup>b,c</sup>, Ting-Shan Chan<sup>d</sup>, Carlos Escudero<sup>e</sup>, Patricia Concepción<sup>a,\*</sup>, Avelino Corma<sup>a,\*</sup>

<sup>a</sup> *Instituto de Tecnología Química, Universitat Politècnica de València-Consejo Superior de Investigaciones Científicas (UPV-CSIC), Avenida de los Naranjos s/n, 46022 Valencia, Spain*

<sup>b</sup> *Department of Physics, Tamkang University, Tamsui 25137 New Taipei City, Taiwan*

<sup>c</sup> *Research Center for X-Ray Science, Tamkang University, Tamsui 25137, New Taipei City, Taiwan*

<sup>d</sup> *National Synchrotron Radiation Research Center, Hsinchu 30076, Taiwan*

<sup>e</sup> *ALBA Synchrotron Light Source, Carrer de la Llum 2-26, 08290 Cerdanyola del Vallès, Spain*

▪ **ABSTRACT**

Ruthenium nanoparticles with a core-shell structure formed by a core of metallic ruthenium and a shell of ruthenium carbide have been synthesized by a mild and easy hydrothermal treatment. The dual structure and composition of the nanoparticles have been determined by synchrotron X-ray Photoelectron Spectroscopy (XPS), Near Edge X-ray Absorption Fine Structure (NEXAFS) analysis and Transmission Electron Microscopy (TEM) imaging. According to depth profile synchrotron XPS and X-Ray Diffraction (XRD) analysis, metallic ruthenium species predominate in the inner layers of the material being ruthenium carbide species located on the upper surface layers. The Ruthenium carbon catalysts presented herein are able to activate both CO<sub>2</sub> and H<sub>2</sub>, exhibiting exceptional high activity for CO<sub>2</sub> hydrogenation at low temperatures (160-200 °C) with 100% selectivity to methane, surpassing by far the most active Ru catalysts reported up to now. Based on catalytic studies and isotopic <sup>13</sup>CO/<sup>12</sup>CO<sub>2</sub>/H<sub>2</sub> experiments, the active sites responsible for this unprecedented activity can be associated to surface ruthenium carbide (RuC) species, which enable CO<sub>2</sub> activation and transformation to methane *via* direct CO<sub>2</sub> hydrogenation mechanism. Both, the high activity and the absence of CO in the gas effluent confer relevance on these catalysts for the Sabatier reaction, a chemical process with renewed interest for storing surplus renewable energy in the form of methane.

**Keywords** Ruthenium carbide, CO<sub>2</sub> activation, low temperature Sabatier, NEXAFS, synchrotron XPS, methane, hydrothermal synthesis, isotopic experiments.

## ▪ INTRODUCTION

The CO<sub>2</sub> concentration in the atmosphere has been growing exponentially in the last decade exceeding the 400 ppm in 2016 and leading to important environmental damages as, for instance, the global warming or sea water acidification.<sup>1</sup> Therefore, the reduction of CO<sub>2</sub> emissions is strongly required. Among the processes reported for CO<sub>2</sub> capture and use, CO<sub>2</sub> methanation reaction (so called Sabatier reaction) has received renewed interest in the last years as a way to store surplus renewable energy in the form of CH<sub>4</sub>, which is easily stored, transported and used in the actual industrial infrastructure.<sup>2</sup> CO<sub>2</sub> methanation is a simple reaction, favoured thermodynamically at low temperatures (CO<sub>2</sub>+ 4H<sub>2</sub> ↔ CH<sub>4</sub> + 2H<sub>2</sub>O; ΔH = -252.9 KJ·mol<sup>-1</sup>), but limited kinetically because of the high CO<sub>2</sub> stability. The catalysts proposed in patents and in the literature for producing CH<sub>4</sub> from CO<sub>2</sub> are based on metals like Ni, Ru, Pd, Rh, mono or multimetallic, with or without promoters (Na, K, Cs, rare-earth elements...) on different supports (TiO<sub>2</sub>, SiO<sub>2</sub>, Al<sub>2</sub>O<sub>3</sub>, CeO<sub>2</sub>, ZrO<sub>2</sub>, CNT doped with N).<sup>3-5</sup> In all cases high temperatures (300-500 °C) are employed which results in large energy input, high operational costs for large-scale production and negative impact on catalyst stability. Ru is a highly active metal for CO<sub>2</sub> methanation at lower temperature, however the highest space time yield to methane reported up to now does not exceed 0.9 μmol<sub>CH<sub>4</sub></sub>·s<sup>-1</sup>·g<sub>cat</sub><sup>-1</sup> at 165 °C and 2.6 μmol<sub>CH<sub>4</sub></sub>·s<sup>-1</sup>·g<sub>cat</sub><sup>-1</sup> at 200 °C and atmospheric pressure, obtained at a 1.6 mL·g<sup>-1</sup>·s<sup>-1</sup> gas feed rate on a Ru/TiO<sub>2</sub> catalyst, still too low for industrial application.<sup>6,7</sup> Therefore, a breakthrough in the CO<sub>2</sub> methanation reaction will require a highly active and selective catalyst able to operate under mild reaction conditions.

Transition metal carbides appear as appealing catalytic alternatives with interesting properties for many processes, such as isomerization of n-heptane,<sup>8</sup> steam reforming of methanol,<sup>9</sup> dry reforming of methane,<sup>10</sup> CO hydrogenation,<sup>11-13</sup> and CO<sub>2</sub> hydrogenation.<sup>14-18</sup> Molybdenum carbide (β-Mo<sub>2</sub>C)<sup>14</sup> and metal supported carbides (Me/Mo<sub>2</sub>C<sup>17</sup> Me = Ni, Co, Cu; or Me/TiC<sup>16</sup> Me = Cu, Ni, Au) have shown high activity for CO<sub>2</sub> hydrogenation (i.e. 6-8% CO<sub>2</sub> conversion at 200 °C, 20 bar and 2.5 mL·g<sup>-1</sup>·s<sup>-1</sup> gas feed rate),<sup>17</sup> being 3-5 times higher than the corresponding metals supported on conventional oxide supports. However, the selectivity to the target product is relatively low (29% and 42% CH<sub>4</sub> at 200 °C on β-Mo<sub>2</sub>C and Ni/Mo<sub>2</sub>C respectively)<sup>17</sup> due to CO formation (39% and 37%, respectively). The high activity has been ascribed to the intrinsic activity of metal carbides to adsorb and activate the CO<sub>2</sub> molecule through a net charge transfer from carbide to the CO<sub>2</sub> molecule.<sup>15,19</sup> The reactivity, i.e. C-O bond cleavage of the CO<sub>2</sub> molecule, strongly depends on the carbon/metal ratio. Thus, CO<sub>2</sub> dissociation occurs spontaneously on a Mo-terminated β-Mo<sub>2</sub>C surface yielding CO and O, while

on a carbon rich surface (i.e.  $\delta$ -MoC) a HOCO intermediate is formed, resulting in different product selectivity.

In an early study, Moreno-Castilla *et al*<sup>20</sup> reported the formation of ruthenium carbide (RuC) in a Ru activated carbon catalyst prepared by sublimating Ru<sub>3</sub>(CO)<sub>12</sub> on a carbon support, followed by thermal decarbonylation in He at 150 °C. Based on CO and H<sub>2</sub> chemisorption data, they argued the formation of a Ru<sup>IV</sup> active phase, which according to the authors has been assigned to RuC. This result has to be reviewed considering the low tendency of ruthenium to form carbides or solid solution with carbon, usually requiring elevated pressure (5 GPa) and temperatures (1700-2500 °C) for their synthesis.<sup>21-24</sup> Moreover, the reported yield to methane in the CO<sub>2</sub>/H<sub>2</sub> reaction was not higher (~1.4-1.0 times) than that of a similar sample without carbide species, which makes the assignation to RuC doubtful.

In the present work, we show the possibility of synthesizing a ruthenium carbide catalyst (labelled as Ru@C) by an easy and mild hydrothermal method instead of using the harsh treatments previously reported. Most importantly, the as synthesized Ru@C catalyst show unprecedented activity for the low temperature (160-200 °C) CO<sub>2</sub> hydrogenation reaction to CH<sub>4</sub>. Methane yields up to 3.5  $\mu\text{mol}_{\text{CH}_4}\cdot\text{s}^{-1}\cdot\text{g}_{\text{cat}}^{-1}$  at 160 °C and 13.8  $\mu\text{mol}_{\text{CH}_4}\cdot\text{s}^{-1}\cdot\text{g}_{\text{cat}}^{-1}$  at 200 °C are achieved at atmospheric pressure and at 8.3 mL·g<sup>-1</sup>·s<sup>-1</sup> feed rate, surpassing by far the most active Ru catalyst reported up to now.<sup>5,6,7,25-26</sup> The catalyst also show good stability under operational conditions with CH<sub>4</sub> selectivity above 99.9%. Finally, we will show that the formation of CH<sub>4</sub> is taken place by direct activation and hydrogenation of CO<sub>2</sub>.

## ▪ EXPERIMENTAL SECTION

### Synthesis of Ru@C-EDTA

Samples with different Ru contents were prepared using the same synthetic procedure but modifying the amount of Ru precursor. In general: X (X = 1.5, 3.1, 5.3 and 6.6) g Ru(acac)<sub>3</sub> (Aldrich), 1.77 g Na<sub>2</sub>EDTA·2H<sub>2</sub>O (Aldrich) and 0.39 g NaOH (Acros) were dissolved in 8 mL of deionized water. Then 4 mL of methanol were added to the mixed aqueous solution under stirring at room temperature, resulting in a red suspension, which was transferred into a 35 mL Teflon-coated stainless steel autoclave followed by static hydrothermal processing at 200 °C for 24 h. After it, the autoclave was taken out of the oven and cooled down to room temperature for 3 h. The generated precipitate was filtered and washed with deionized water and acetone for five times. Samples were labelled as Ru@C-EDTA-X, where X corresponds to the ruthenium loading, determined by ICP (Table S1).

### Synthesis of Ru@C-Glucose

120 mg of glucose (Aldrich) dissolved in 7 mL of deionized water were stirred at room temperature for 0.5 h. Then 100 mg of RuO<sub>2</sub> (Aldrich, 99.9%, particle size 32 nm, determined by XRD) were added and mixed under ultra-sonication (Branson 3510 operating at 40 Hz) for 0.5 h, obtaining a black suspension. The so obtained suspension was transferred into a Teflon-coated stainless steel autoclave of 12.5 mL. The autoclave was introduced in an oven placed at 175 °C and kept for 18 h under static conditions. After it, the autoclave was taken out of the oven and cooled down to room temperature for 2 h. The content of the autoclave was then filtrated under vacuum conditions, recovering a black solid. The solid was washed five times first with water and later with acetone. Finally, it was dried in an oven at 60 °C for 12 h. The loading of ruthenium in the sample was 24.3 wt %, according to ICP analysis.

#### **Synthesis of Ru/C-WI**

The sample was prepared by a wet impregnation method as follows: 396 mg of Ru(acac)<sub>3</sub> were dissolved in 20 mL toluene for 0.5 h. Then 900 mg of carbon (activated charcoal Norit®, Aldrich) were added and stirred for 15 h at room temperature. The final suspension was evaporated under vacuum resulting in a black solid. The solid was reduced in 50 mL·min<sup>-1</sup> H<sub>2</sub> at 250 °C for 3 h with a heating ramp of 10 °C·min<sup>-1</sup>, followed by cooling down in N<sub>2</sub> to 25 °C. After this, it was oxidized in 50 mL·min<sup>-1</sup> O<sub>2</sub> flow at 400 °C for 3 h. The loading of ruthenium in the sample was 3.0 wt %, according to ICP analysis. XRD is shown in Figure S5.

#### **Synthesis of Ru/C-Ar800**

58 mg of Ru(acac)<sub>3</sub> were dissolved in 20 mL of acetone and stirred at 50 °C. 1.47 g of Na<sub>2</sub>EDTA and 0.12 g NaOH were dissolved in water (20 mL) and the resulting aqueous solution was added to the metal solution and stirred at 50 °C for 0.5 h. Then, 1.6 g of carbon (activated charcoal Norit®, Aldrich) were added and the mixture was refluxed at 50 °C for 24 h. After cooling, the suspension was rotoevaporated, washed with water, filtered and dried at 100 °C overnight. The black solid was pyrolyzed in an Ar flow (10 mL·min<sup>-1</sup>) at 800 °C for 5 h (5 °C·min<sup>-1</sup>). XRD is shown in Fig. S5.

#### **Synthesis of Ru@C/NG**

The catalyst was synthesized according to Reference 27. Briefly, graphene oxide (GO) support was prepared following the improved Hummers method. GO was doped with nitrogen using formaldehyde (37% in water, Aldrich) and melamine (Acros) and the suspension was transferred into a Teflon-coated stainless steel autoclave (12.5 mL) and kept at 180 °C for 12 h. The gel obtained was submitted to pyrolysis in a N<sub>2</sub> flow at 750 °C for 5 h. NG support was dispersed in a phosphate buffered solution with the metal precursor (RuCl<sub>3</sub>·3H<sub>2</sub>O, Johnson Matthey), dopamine hydrochloride (Aldrich) and CTAB (Acros) and hydrothermally treated at 140 °C for 6

h. The resulting suspension was centrifuged and the solid was washed with water and dried. The catalyst was obtained after a high temperature treatment in argon (800 °C, 10 mL·min<sup>-1</sup>) for 3 h.

#### **Ruthenium references**

Commercial Ru on carbon, **Ru/C-com** (Acros Organics, 5 wt % Ru) and **Ru-Black** (Aldrich, >98%) were used as reference samples in catalytic and spectroscopic studies. XRD are shown in Figure S5.

#### **Catalysts characterization**

The Ru content was analysed by Inductively Coupled Plasma Optical Emission Spectrometry (ICP-OES) using a Varian 715-ES spectrometer. The samples were dissolved in aqua regia at 60 °C for 20 h. X-Ray powder diffraction (XRD) was recorded with a Philips X'Pert diffractometer using a monochromatic Cu K $\alpha$  radiation ( $\lambda=0.15406$  nm). Average particle size was calculated from the main peaks (38.4, 42.2, 44.0, 58.3, 69.4, 78.4;  $2\theta$ ) of Ru<sup>0</sup> (JCPDS: 00-006-0663) using the Scherrer equation and assuming a shape factor  $k=0.9$ . Transmission Electron Microscopy (TEM) measurements were performed in a JEOL-JEM 2100F operating at 200 kV. Samples were prepared by dropping the suspension of the powder catalyst using ethanol as the solvent directly onto holey-carbon coated Cu grids. The amount of surface ruthenium metal sites was measured by CO chemisorption at 25 °C in a Quantachrome Autosorb-1C instrument by extrapolating the total gas uptakes in the adsorption isotherms at zero pressure and assuming an adsorption stoichiometry of 1:1 (Ru:CO).<sup>20</sup> Before measurements, about 300 mg of catalyst were activated in a helium flow at 100 °C (2 h) and in vacuum at the same temperature (1 h). Near Edge X-ray Absorption Fine Structure (NEXAFS) spectra at Ru  $L_3/L_2$  edge were collected by the total fluorescence yield *via* Lytle detector at beamline 16A1 at Taiwan Light Source. The spot size was 0.5 x 0.5 (HxV) mm<sup>2</sup>, where probed at the Ru powder sample by incident 45° angle. X-ray energy from Si (111) monochromator was calibrated using the energy jump of standard Mo foil at  $L_3$  edge. Synchrotron X-ray Photoelectron Spectroscopy (XPS) experiments were performed at beamline BL24-CIRCE (NAPP branch) at ALBA Synchrotron Light Source (Cerdanyola del Vallès, Barcelona). CIRCE is an undulator beamline with a photon energy range of 100-2000 eV. Data acquisition was performed using a PHOIBOS 150NAP electron energy analyser (SPECS GmbH). The spectra were acquired with exit slit of 20  $\mu$ m and pass energy of 20 eV. The X-ray spot size was 100  $\mu$ m x 65  $\mu$ m (HxV). Incident photon energies of 500 and 1150 eV for Ru 3d and C 1s were used to record the XPS spectra. Binding energies (BE) were calibrated with respect to C 1s signal settled at 284.5 eV. The sample (50 mg) was pelletized, mounted onto the sample holder and measured at room temperature at a 10<sup>-9</sup> mbar pressure without previous activation. Shirley type background and Lorentzian type curves have been used in the spectra fitting. Laboratory X-ray Photoelectron Spectroscopy (XPS) experiments were performed on a SPECS equipment

with a Phoibos 150 MCD-9 detector and using non-monochromatic AlK $\alpha$  (1486.6 eV) X-ray radiation. The pass energy was 20 eV and the X-ray power was 100 W. Raman studies were performed using a Renishaw “In via” spectrometer connected to an Olympus Microscope. The instrument is equipped with a He-Ne green laser (514 nm), a diode laser (785 nm) and a CCD detector. Temperature Programmed Reduction with H<sub>2</sub> (TPR-H<sub>2</sub>) studies were performed using a quartz reactor, connected online to a mass spectrometer Balzer (QMG 220M1). 120 mg of catalyst were flushed with Argon at 25 °C for 30 min, and then switched to a 70 vol % H<sub>2</sub> in Ar flow (14 mL·min<sup>-1</sup>). The reaction was carried out at increasing temperatures (160, 180, 200, 220, 260 and 280 °C, at a rate of 10 °C·min<sup>-1</sup>). The *m/z* values used to monitor each product were 44 (CO<sub>2</sub>), 28 (CO and CO<sub>2</sub>), 2 (H<sub>2</sub>), 15 (CH<sub>4</sub>), 16 (CH<sub>4</sub>) and 18 (H<sub>2</sub>O).

#### **Isotopic <sup>13</sup>CO/<sup>12</sup>CO<sub>2</sub>/H<sub>2</sub> experiments**

Catalytic tests with carbon labelled species were performed in a home-made stainless steel cell connected online with a mass spectrometer (Balzer QMG 220M1). The catalysts (15 mg) were pelletized and kept in vacuum at 120 °C for 0.5 h. In case of Ru/C-com, the sample was additionally reduced *in situ* with a H<sub>2</sub> flow (280 °C, 1 h, 10 mL·min<sup>-1</sup>) before reaction. After activation, a mixture of <sup>13</sup>CO/<sup>12</sup>CO<sub>2</sub>/H<sub>2</sub> (1:1:6 vol %) was fed continuously at 15 mbar total pressure. Then, the temperature was increased to 160 °C and finally the pressure was set at 25 mbar. The reaction evolution was monitored by Mass Spectrometry (MS) with *m/z* values: 44 (<sup>12</sup>CO<sub>2</sub>), 45 (<sup>13</sup>CO<sub>2</sub>), 28 (<sup>12</sup>CO), 29 (<sup>13</sup>CO), 15 (<sup>12</sup>CH<sub>4</sub>), 17 (<sup>13</sup>CH<sub>4</sub>), 18 (H<sub>2</sub>O) and 2 (H<sub>2</sub>).

#### **CO<sub>2</sub> hydrogenation catalysis**

CO<sub>2</sub> hydrogenation was performed in a stainless steel fixed bed reactor with an inner diameter of 11 mm and 240 mm length. Typically, 210 mg of catalyst (particle size 400-600  $\mu$ m) were diluted in SiC in a weight ratio 0.14 (Cat/SiC). Ru@C-EDTA and Ru@C-Glucose were not activated before reaction, while the other samples were *in situ* reduced prior to catalytic tests (25 mL·min<sup>-1</sup> H<sub>2</sub>, 280 °C, 1 h, 10 °C·min<sup>-1</sup>). The reaction took place at atmospheric pressure and the reaction temperatures were 160, 180 and 200 °C. Each temperature was maintained for at least 1.5 h. The reaction was carried out at 21428 h<sup>-1</sup> GHSV under concentrated (23.8 vol % CO<sub>2</sub>, 71.3 vol % H<sub>2</sub>, 5 vol % N<sub>2</sub>) or diluted (5 vol % CO<sub>2</sub>, 20 vol % H<sub>2</sub>, 75 % vol N<sub>2</sub>) conditions. Direct analysis of the reaction products was done by online gas chromatography (GC), using a SCION-456-GC equipment with TCD (MS-13X column) and FID (BR-Q Plot column) detectors. Blank experiments (in the presence of SiC) shown the absence of homogeneous contribution to the reaction. Turnover frequency values (TOFs) were obtained from CO chemisorption data.

#### **CO hydrogenation catalysis**

CO hydrogenation was performed in the CO<sub>2</sub> hydrogenation reactor setup described before. In this case, the inlet gas mixture was 30 % vol CO, 60 % vol H<sub>2</sub> and 10 % vol Ar with identical

total flow ( $100 \text{ mL}\cdot\text{min}^{-1}$ ). The process took place at atmospheric pressure and in a temperature range of  $160\text{-}240 \text{ }^\circ\text{C}$ , using 210 mg of catalyst.

## ▪ RESULTS AND DISCUSSION

The Ru@C-EDTA samples are prepared under hydrothermal conditions (details in Experimental Section), modifying the amount of Ruthenium(III) acetylacetonate ( $\text{Ru}(\text{acac})_3$ ) in the synthesis gel, while keeping constant the ethylenediaminetetraacetic acid disodium salt dihydrate ( $\text{Na}_2\text{EDTA}\cdot 2\text{H}_2\text{O}$ ). The synthesis takes place at autogenous pressure at  $200 \text{ }^\circ\text{C}$  for 24 h. The ruthenium loading in the as prepared samples, determined from ICP analysis, takes values between 6 wt % and 28 wt % (Table S1). Representative TEM images obtained from the Ru@C-EDTA samples are presented in Figure 1 and Fig.S1-S4, which show the presence of  $\text{Ru}^0$  NP embedded in a carbon matrix. An homogeneous distribution of small Ru NP with average particle sizes of 2-5 nm are observed in the Ru@C-EDTA-6, Ru@C-EDTA-12 and Ru@C-EDTA-20 samples. However, a more heterogeneous size distribution of small (2-5 nm) and bigger (10-15 nm) Ru nanoparticles can be detected in the Ru@C-EDTA-28 sample (Fig.S4).

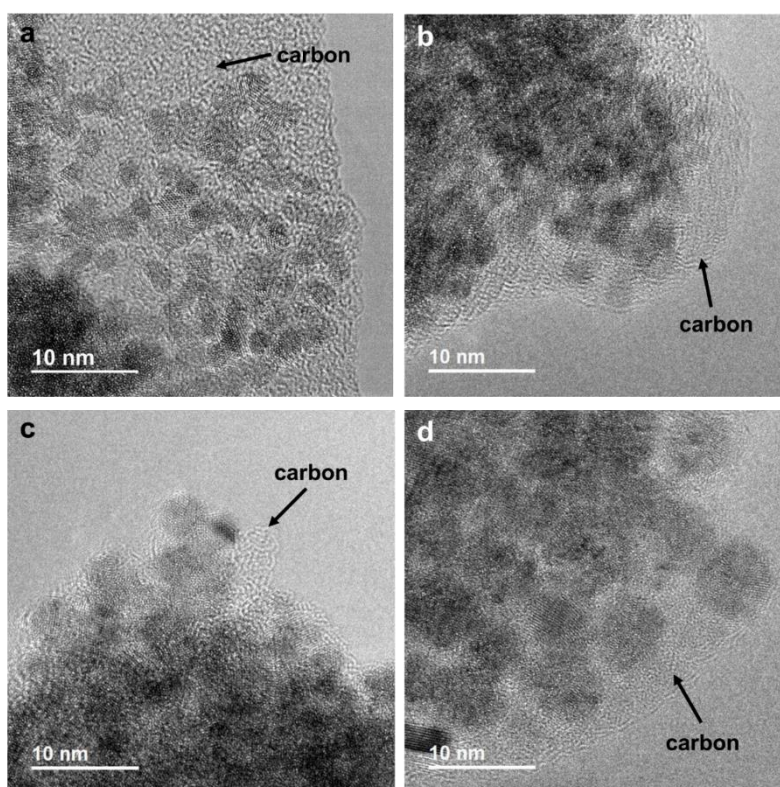


**Figure 1.** TEM images of Ru@C-EDTA samples prepared by hydrothermal synthesis with different ratios of Ru/EDTA. (a) Ru@C-EDTA-6, (b) Ru@C-EDTA-12, (c) Ru@C-EDTA-20 and (d) Ru@C-EDTA-28.

This is in accordance with the bulk information extracted from X-ray diffractograms (Fig.S5) where the peak broadening observed in samples Ru@C-EDTA-6, Ru@C-EDTA-12 and Ru@C-EDTA-20 samples corresponds to a small crystallite size, whereas some sharp peaks are visualized in the Ru@C-EDTA-28 sample, corresponding to crystalline Ru<sup>0</sup> (hexagonal, JCPDS: 00-006-0663). The nature of the carbon matrix studied by Raman spectroscopy shows a graphitic structure (1600 cm<sup>-1</sup>) with defects (1371 cm<sup>-1</sup>) and some amorphous carbon (1506 cm<sup>-1</sup>)<sup>29</sup> (Fig.S6). In addition, concerning to the nature of ruthenium species, XPS studies performed in a laboratory scale spectrometer using AlK $\alpha$  (1486.6 eV) X-ray energy (Fig.S7) displays the presence of Ru<sup>0</sup> (279.3 eV) and RuO<sub>2</sub> (281.0 eV). However, high-resolution XPS spectroscopy using synchrotron radiation allowed us to obtain surface sensitive information of the Ru@C-EDTA samples working at variable X-Ray excitation energy. In fact, at low X-ray excitation energy (500 eV) with a probing depth of around 2.2 nm,<sup>30</sup> an additional ruthenium specie at 279.6 eV, together with Ru<sup>0</sup> (at 279.1 eV) and RuO<sub>2</sub> (281.0-280.4 eV) are clearly observed (Fig.2a). The surface concentration of this new specie slightly increases from ~56% to ~70% at decreasing the Ru content in the samples (Fig.2b).

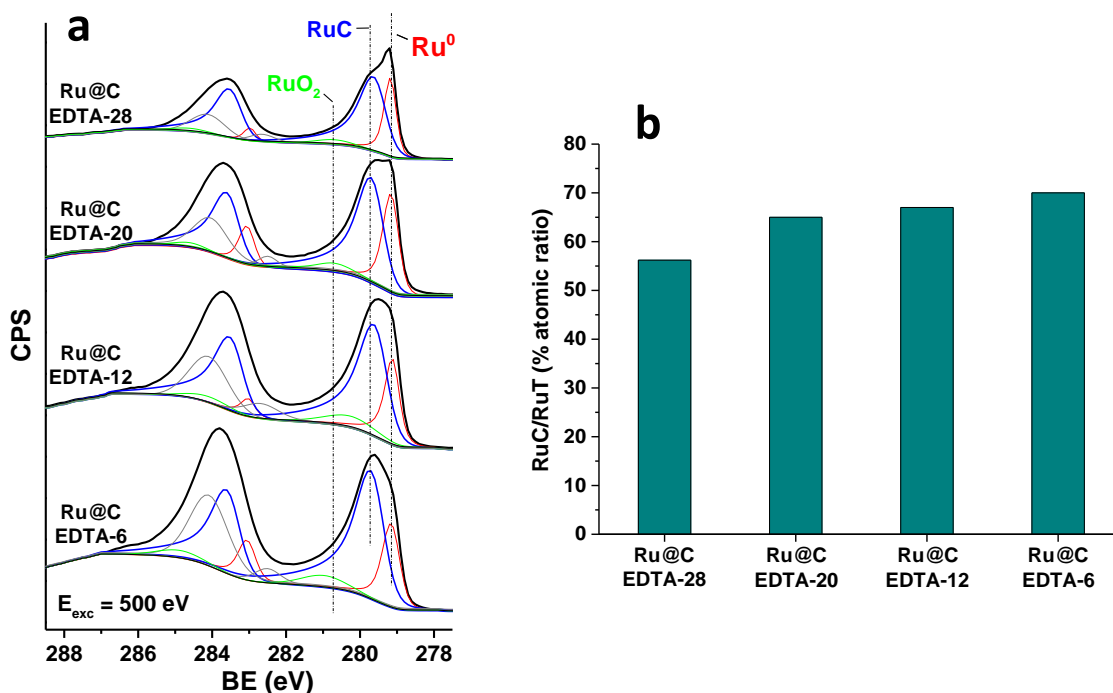


**Figure 2.** a) Synchrotron XPS of the C 1s and Ru 3d<sub>5/2</sub> core levels at 500 eV X-ray excitation energy on fresh Ru@C-EDTA samples. Colour code for components: Ru<sup>0</sup> (red), RuC (blue) RuO<sub>2</sub> (green), C (grey). b) Surface concentration of the RuC phase relative to the total Ru (RuT).

Based on XPS depth profile analysis at a sample depth of 4.4 nm, the contribution of the new component at 279.6 eV to the total Ru peak intensity decreases ~ 30-40% in all samples at the

expense of the component of Ru<sup>0</sup> (Fig.S8), meaning that the new Ru specie identified by synchrotron XPS is preferentially located on the upper surface layers of the catalyst. This new component is ascribed in our work to ruthenium carbide (RuC) species. However, their assignation is not straightforward, due to the lack of reference data associated with RuC and uncertainties that exist in the literature regarding to the assignation of ruthenium chemical states.<sup>31</sup> Our assignation has been made based on previous studies where a +0.5 eV shift respect to the metal was related to carbide species,<sup>32</sup> and is also supported by HRTEM analysis (Fig.3a and Fig.S9), in where lattice fringes at 0.21 and 0.31 nm, corresponding to Ru<sup>0</sup> and RuO<sub>x</sub> respectively, and 0.28 nm, due to RuC (PDF number 01-089-3016) are detected. In addition to XPS and HRTEM analysis, the assignation of the new detected specie to RuC is supported by Near-Edge X-ray Absorption Fine Structure (NEXAFS) technique performed on the Ru@C-EDTA-20 sample at the Ru L<sub>2,3</sub>-edge, which is compared with RuO<sub>2</sub> and Ru<sup>0</sup> references (Fig.3b). The spectra reflect the electronic structure of surface Ru species and their local environment, which don't correspond to RuO<sub>2</sub> nor Ru<sup>0</sup>. Indeed, the Ru L<sub>2,3</sub>-edge white lines of Ru@C-EDTA-20 (located around 2840 and 2969 eV for the L<sub>3</sub> and L<sub>2</sub>, respectively) are shifted to higher photon energy compared to that of Ru metal, and to lower energy respect to that of RuO<sub>2</sub>, while are compatible with the RuC phase.<sup>34</sup> Moreover, the global spectral shapes characteristic of Ru<sup>0</sup> and RuO<sub>2</sub> result incompatible with the spectra collected on the Ru@C-EDTA-20 sample, where both the double peak structure around 2850 (L<sub>3</sub>) / 2980 (L<sub>2</sub>) eV (characteristic of the metal phase) and the one broadened peak structure of the white line (characteristic of the RuO<sub>2</sub> phase) are absent (details in Fig.S10(a),(b)). **Curve fitting simulation from the NEXAFS spectra at L<sub>3</sub> and L<sub>2</sub> edge is shown in Figure 3c, representing two peaks corresponding to the electronic transition 2p->4d-t<sub>2g</sub> (A) and 4d-e<sub>g</sub> (B) state. The A/B ratios in RuO<sub>2</sub> and Ru metal at L<sub>3</sub> edge (L<sub>2</sub>) are 0.024 (0.17) and 2.61 (2.92) respectively, which are the opposite cases by their electronic configurations (4d<sup>4</sup> and 4d<sup>8</sup> electrons). In the Ru@C-EDTA-20 sample, the A/B ratios result at L<sub>3</sub> edge (1.19) and L<sub>2</sub> edge (2.00), which is between RuO<sub>2</sub> and Ru metal, reflecting a different feature symmetry and ligand environment in the Ru@C-EDTA sample.** This agrees with the previous results and indicates that the upper surface of our catalysts is most likely ascribed to RuC. To our knowledge, this is the first time that a ruthenium carbide phase is formed under mild conditions (hydrothermal synthesis at 200 °C) in opposite to the harsh conditions (5 GPa and 1000-2500 °C) usually required for its synthesis.<sup>21-24</sup>

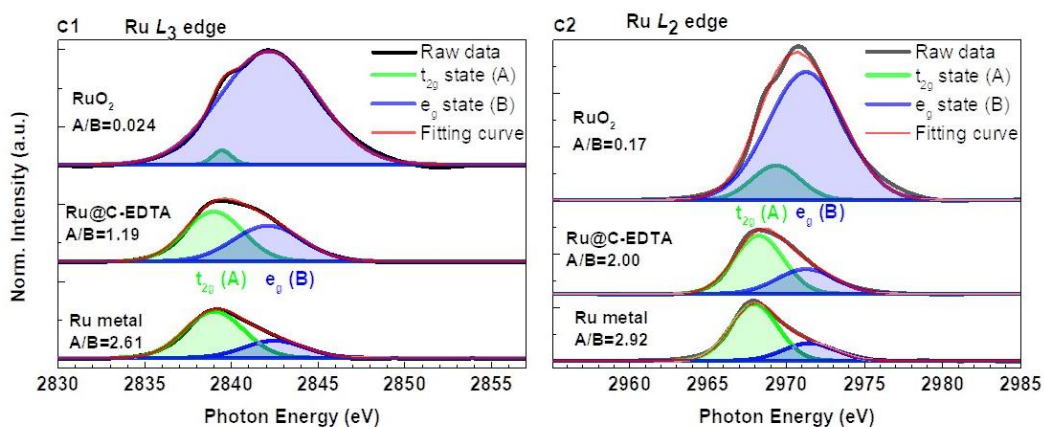
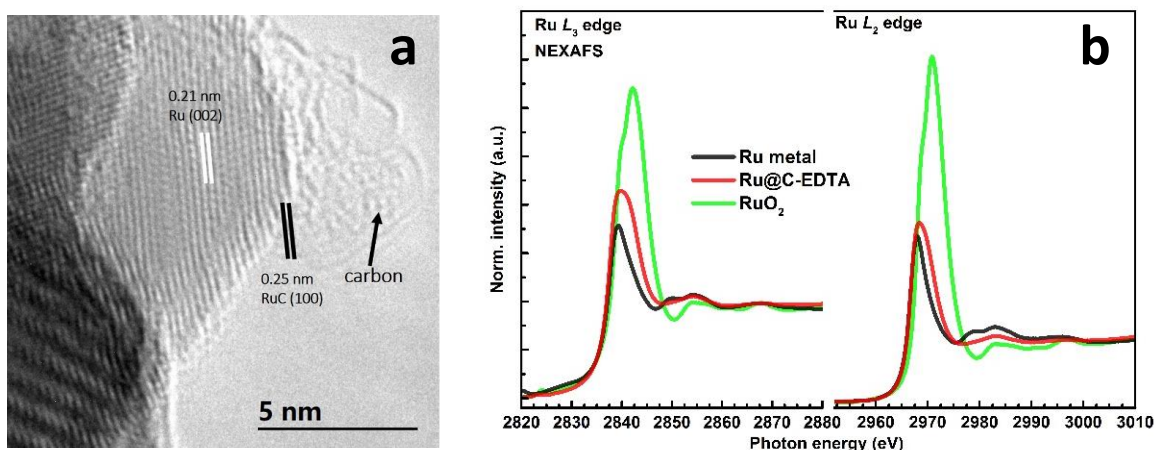


**Figure 3.** (a) HRTEM image of the Ru@C-EDTA-20 sample. (b)  $L_3$ -edge spectra (left panel) and  $L_2$ -edge spectra (right panel) of  $\text{Ru}^0$ , Ru@C-EDTA-20, and  $\text{RuO}_2$ . (c) **Curve fitting simulation from the NEXAFS spectra at  $L_3$  and  $L_2$  edge on  $\text{RuO}_2$ , Ru@C-EDTA-20 and  $\text{Ru}^0$ .**

From the point of view of their application in the  $\text{CO}_2$  hydrogenation reaction, an important issue to deal with is the thermal stability of the Ru@C-EDTA catalytic systems under  $\text{H}_2$  rich conditions, which is proved by a TPR- $\text{H}_2$  study. In this experiment, performed in  $\text{H}_2$  flow at atmospheric pressure, the  $\text{CH}_4$  formation (due to carbide and/or carbon hydrogenation) is followed by online Mass Spectrometry (MS). Under these conditions,  $\text{CH}_4$  MS signal ( $m/z=15$ ) clearly evolves above  $240^\circ\text{C}$  (Fig.S11), limiting the catalytic studies to this temperature.

The herein reported Ru@C-EDTA catalysts show markedly high activity at low temperature ( $160\text{--}200^\circ\text{C}$ ) and atmospheric pressure for the  $\text{CO}_2$  hydrogenation reaction, with 99.9% selectivity to methane, operating at  $21428\text{ h}^{-1}$  GHSV (details in Experimental Section). The  $\text{CO}_2$  conversion and the methane space time yield ( $\text{STY}_{\text{CH}_4}$ ) in the  $160\text{--}180^\circ\text{C}$  temperature range at concentrated reaction conditions is summarized in Table 1a, where an increase in the catalytic activity is observed at increasing Ru loading in the samples. The catalyst stability of Ru@C-EDTA-

20 sample tested over a period of ~15 h reaction time at 160 °C is plotted in Figure 4. A decrease in activity (~8%) is observed in the first 12 h of reaction, while it remains stable in the last 3 h. The observed loss of activity corresponds to a partial removal of surface ruthenium carbide species under reaction conditions, as evidenced from XPS studies using synchrotron radiation performed on the spent catalysts (Fig.S12a) **while maintaining the carbonaceous matrix where the Ru NPs are embedded (see Raman spectra of the spent catalysts in Fig.S6)**. In fact, a loss of RuC species is observed in all samples according to the XPS spectra acquired at 500 eV X-ray excitation energy, being in the order of 31-23% on the Ru@C-EDTA-6, Ru@C-EDTA-12 and Ru@C-EDTA-20 samples and of 5% on the Ru@C-EDTA-28 sample (Fig.S12b). Based on this data, a fairly good correlation between the amount of surface RuC of the spent Ru@C-EDTA catalysts and the  $STY_{CH_4}$  at 160 °C (Table 1a) is found, as displayed in Figure 5. These results suggest that the RuC species should play a key role in the catalytic activity of the Ru@C-EDTA samples, as discussed later.

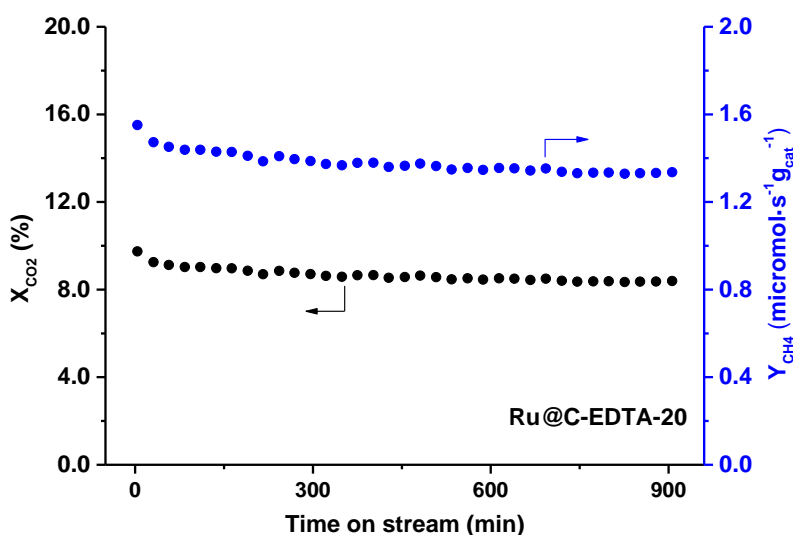


**Figure 4.**  $CO_2$  conversion (left axe, black) and methane STY (right axe, blue) on the Ru@C-EDTA-20 catalyst at 160 °C, 21428  $h^{-1}$  GHSV and 5%  $CO_2$ , 20%  $H_2$  and 75%  $N_2$  (% vol).

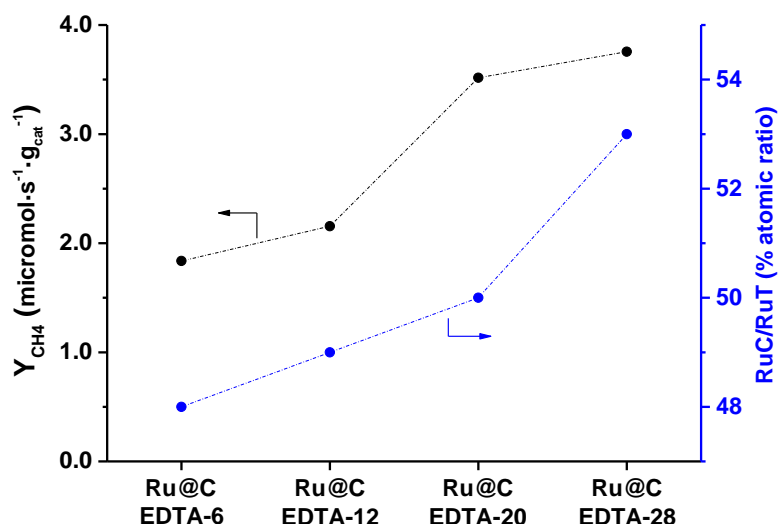


**Figure 5.** Methane STY (left axe, black) at 160 °C, 21428 h<sup>-1</sup> GHSV and 23.8% CO<sub>2</sub>, 71.3% H<sub>2</sub>, 5% N<sub>2</sub> (% vol). On the right axe (blue), RuC/RuT atomic ratio obtained from XPS analysis on the spent Ru@C-EDTA catalysts at 500 eV X-ray excitation energy (Fig.S12).

The activity of the Ru@C-EDTA samples surpasses by far that of other synthesized ruthenium carbon catalysts as shown in Table 1b and is markedly higher than that of most active ruthenium catalysts we found in the literature (Table S2). Being aware that the CO<sub>2</sub> methanation on Ru catalysts has been reported to be size dependent, where large particles were found to be more active than smaller ones,<sup>35</sup> reference catalysts with different particle sizes have been considered. All catalysts prepared by different synthesis strategies, some of them reproducing those of the literature,<sup>20,27,36</sup> and the commercial type catalysts (such as Ru/C-com and Ru-Black) show negligible activity at the mild operation conditions considered in this work. Moreover, the selectivity to methane is almost 100 % on the Ru@C-EDTA samples, while other by-products like CO or C<sub>x</sub>H<sub>y</sub> are formed on the other samples (Fig.S13). Altogether endows in a very promising catalyst for the Sabatier reaction. In addition, the synthesis of this type of catalyst can be also achieved starting from other precursors like RuO<sub>2</sub> and glucose, using water as solvent (see Experimental Section and Fig.S14). The similar catalytic activity achieved in the Ru@C-Glucose catalyst, (see Table S3) allows to discard the enhanced catalytic activity of the Ru@C-EDTA catalysts due to the presence of nitrogen or Na<sup>+</sup> additives coming from the Na<sub>2</sub>EDTA precursor.

Regarding to the ruthenium surface speciation in the samples, Ru<sup>0</sup> is the only specie present in all reference catalysts (Table 1b). However, in Ru@C-EDTA materials, it exists a combination of Ru<sup>0</sup> and RuC (that predominates in upper layers), together with carbon coating, which could explain their much superior performance. In fact, if the RuC phase in Ru@C-EDTA-20 is removed by treating the catalyst in H<sub>2</sub> at 280 °C, the catalytic activity strongly decreases (Fig.S15). This

result reinforces our previous assumption of RuC species as a key component responsible for the high catalytic reactivity obtained in the CO<sub>2</sub> methanation reaction at low temperature.

**Table 1. a) Catalytic activity in the CO<sub>2</sub> hydrogenation reaction at concentrated reaction conditions<sup>a</sup> on the Ru@C-EDTA samples; b) Catalytic activity at 160 °C of the Ru@C-EDTA-20 sample compared to other reference ruthenium carbon samples.**

a)

Sample	160 °C		180 °C	
	X <sub>CO2</sub> (%)	STY <sub>CH4</sub> ( $\mu\text{mol}_{\text{CH}_4}\cdot\text{s}^{-1}\cdot\text{g}_{\text{cat}}^{-1}$ )	X <sub>CO2</sub> (%)	STY <sub>CH4</sub> ( $\mu\text{mol}_{\text{CH}_4}\cdot\text{s}^{-1}\cdot\text{g}_{\text{cat}}^{-1}$ )
Ru@EDTA-28	4.9	3.76	13.2	10.07
Ru@EDTA-20	4.6	3.52	9.8	7.56
Ru@EDTA-12	2.7	2.16	6.5	5.26
Ru@EDTA-6	1.3	1.84	2.5	3.48

b)

Sample	wt% Ru (Part. size) <sup>f</sup>	X <sub>CO2</sub> <sup>a</sup> (%)	STY <sub>CH4</sub> ( $\mu\text{mol}_{\text{CH}_4}\cdot\text{s}^{-1}\cdot\text{g}_{\text{cat}}^{-1}$ )	(%) Selectivity CH <sub>4</sub> / CO / C <sub>2</sub> H <sub>6</sub>
Ru@C-EDTA-20	20.2% (--)	4.6	3.52	99.9 / 0 / 0.1
Ru/C-WI <sup>b</sup>	3.0% (17 nm)	<0.1	0.04	38.3 / 61.5 / 0.2
Ru/C-com	5.0% (2 nm) <sup>g</sup>	<0.1	0.07	92.7 / 6.8 / 0.5
Ru/C-Ar800 <sup>c</sup>	4.0% -	0.1	<0.01	73.4 / 25.6 / 1.0
Ru@C/NG <sup>d</sup>	13.0% <sup>27</sup> -	0	-	-
Ru <sub>3</sub> (CO) <sub>12</sub> /C <sup>e</sup>	2.5% (1.2 nm) <sup>20</sup>	<0.1	0	0 / 100 / 0
Ru-Black Aldrich	100% (20 nm)	0.3	0.23	99.9 / 0 / 0.1

<sup>a</sup>1 bar, GHSV 21428 h<sup>-1</sup>, reactant feed composed of 23.8 vol % CO<sub>2</sub>, 71.2 vol % H<sub>2</sub>, 5 vol % N<sub>2</sub>; <sup>b</sup>Prepared by wet impregnation of Ru(acac)<sub>3</sub> on a carbon support; <sup>c</sup>Prepared by pyrolysis of the metal precursors according to ref. 36; <sup>d</sup>Prepared through thermal annealing of polydopamine (PDA) coated Ru NP supported on a three-dimensional N-doped graphene layer as in ref. 27; <sup>e</sup>Prepared from Ru<sub>3</sub>(CO)<sub>12</sub> precursor as described in ref. 20; <sup>f</sup>Calculated by XRD; <sup>g</sup>Calculated by HRTEM.

The reaction mechanism (direct CO<sub>2</sub> hydrogenation or *via* reverse water gas-shift (RWGS)) of the Ru@C-EDTA samples have been studied combining catalytic studies using a CO/H<sub>2</sub> feed, with isotopic studies using a <sup>13</sup>CO/<sup>12</sup>CO<sub>2</sub>/H<sub>2</sub> (1:1:6) reactant feed. For this purpose, the Ru@C-EDTA-20 catalyst is selected as the reference sample that presents surface RuC species, and its behaviour compared to a sample containing only Ru<sup>0</sup> (i.e. commercial Ru/C-com). Catalytic studies show negligible CO conversion (~0.01-0.05%) on the Ru@C-EDTA-20 sample in the 180-240 °C temperature range, while CO reacts in the commercial Ru/C sample (Table S4). Isotopic studies in the presence of both <sup>13</sup>CO/<sup>12</sup>CO<sub>2</sub> show a very high preferential <sup>12</sup>CO<sub>2</sub> hydrogenation versus <sup>13</sup>CO on the Ru@C-EDTA-20 sample, since only <sup>12</sup>CH<sub>4</sub> is detected (Fig.S16a). Meanwhile, <sup>13</sup>CO is preferentially hydrogenated versus <sup>12</sup>CO<sub>2</sub> on the Ru/C sample, resulting in <sup>13</sup>CH<sub>4</sub> formation (Fig.S16b). Combining both results, and taking into account the different selectivity to CO obtained during the CO<sub>2</sub> hydrogenation, (CO is not detected in the Ru@C-EDTA-20 sample, while it is formed as the major by-product in the Ru/C sample, Fig.S13), we can conclude that a direct CO<sub>2</sub> hydrogenation path to CH<sub>4</sub> takes place on the Ru@C-EDTA-20 sample, while contribution of a RWGS reaction mechanism occurs on the Ru/C sample in the presence of Ru<sup>0</sup>, in agreement to previous studies.<sup>35,37-42</sup> Moreover, the fact that <sup>13</sup>CH<sub>4</sub> is not observed in the isotopic studies of the Ru@C-EDTA-20 sample allows to discard the co-existence of Ru<sup>0</sup> species on the catalyst surface or, if present, they should be in a very low amount, being the activity ascribed predominately to the presence of RuC species. Based on it, a core-shell structure containing a metallic core and an upper shell of ruthenium carbide and carbon species can be proposed in our catalysts. The RuC phase has been proven to be the active specie in the CO<sub>2</sub> hydrogenation, which in accordance with the literature,<sup>15,19</sup> favors CO<sub>2</sub> binding and activation.

## ▪ CONCLUSION

We have described an easy hydrothermal synthesis method that allows the stabilization of surface ruthenium carbide species on a metallic ruthenium core. Advanced surface-sensitive characterization techniques such as synchrotron XPS, NEXAFS and HRTEM were required to elucidate the presence of these carbidic species, which are not present in other catalysts previously reported. Surface RuC enables CO<sub>2</sub> activation, which is hydrogenated to methane in

a direct reaction path, yielding 100% selectivity to CH<sub>4</sub>. The high activity at low temperature (160-200 °C) and the absence of CO in the gas effluent makes the herein synthesized Ru@C-EDTA and Ru@C-Glucose samples very promising candidates for the Sabatier reaction.

#### ▪ ASSOCIATED CONTENT

Supporting Information includes XRD diffractograms of tested materials; Raman spectra of Ru@C-EDTA-20 sample; Laboratory XPS; C 1s and Ru 3d Synchrotron XPS core levels of the Ru@C-EDTA samples; HRTEM images of Ru@C-EDTA samples; NEXAFS experiments; TPR-H<sub>2</sub> profile of Ru@C-EDTA-20; Catalytic results on Sabatier reaction at atmospheric pressure of Ru@C-EDTA-20, RU@C-glucose and other reference samples; State of art in Sabatier reaction; Catalysis with Syngas; Isotopic <sup>13</sup>CO/<sup>12</sup>CO<sub>2</sub> experiments.

#### ▪ AUTHOR INFORMATION

##### Corresponding authors

\*pconcepc@upvnet.upv.es

\*acorma@itq.upv.es

##### ORCID

Patricia Concepción 0000-0003-2058-3103

Avelino Corma 0000-0002-2232-3527

##### Notes

The authors declare no competing financial interest.

#### ▪ ACKNOWLEDGMENTS

The research leading to these results has received funding from the Spanish Ministry of Science, Innovation and Universities through “Severo Ochoa” Excellence Programme (SEV-2016-0683) and the PGC2018-097277-B-100 (MCIU/AEI/FEDER, UE) project. The authors also thank the Microscopy Service of UPV for kind help on measurements. A. García-Ortiz thanks “Severo Ochoa” Programme (SEV-2016-0683) for a predoctoral fellowship. C. H. Chuang acknowledges financial support from MOST project 107-2112-M-032-005. J. Cored thanks the Spanish Government (MINECO) for a “Severo Ochoa” grant (BES-2015-075748). The authors thanks the support of ALBA Synchrotron Light Source staff for the successful performance of the measurements at CIRCE beamline (BL24).

#### ▪ ABBREVIATIONS

CNT, carbon nanotube; acac, acetylacetonate; EDTA, ethylenediaminetetraacetic acid derived salt; CTAB, Cetyl Trimethyl Ammonium Bromide; NP, nanoparticle; wt, weight; vol, volume.

## ▪ REFERENCES

- (1) Yuan, Z.; Eden, M. R.; Gani, R. Toward the Development and Deployment of Large-Scale Carbon Dioxide Capture and Conversion Processes. *Ind. Eng. Chem. Res.* **2016**, *55*, 3383-3419.
- (2) Stangeland, K.; Kalai, D.; Li, H.; Yu, Z. CO<sub>2</sub> Methanation: The Effect of Catalysts and Reaction Conditions. *Energy Procedia* **2017**, *105*, 2022-2027.
- (3) Solis-Garcia, A.; Fierro-Gonzalez, J. C. Mechanistic Insights into the CO<sub>2</sub> Methanation Catalyzed by Supported Metals: A review. *J. Nanosci. Nanotechnol.* **2019**, *19*, 3110-3123.
- (4) Panagiotopoulou, P. Hydrogenation of CO<sub>2</sub> over supported noble metal catalysts. *Appl. Catal. A: Gen.* **2017**, *542*, 63-70.
- (5) Qin, Z.; Zhou, Y.; Jiang, Y.; Liu, Z.; Ji, H. Recent advances in heterogeneous Catalytic Hydrogenation of CO<sub>2</sub> to methane: Chapter 4. In *New Advances in Hydrogenation Processes-Fundamentals and Applications*; <http://dx.doi.org/10.5772/65407> Intechopen: 2017; pp 57-82.
- (6) Kim, A.; Sanchez, C.; Patriarche, G.; Ersen, O.; Moldovan, S.; Wisnet, A.; Sassoey, C.; Debecker, D. P. Selective CO<sub>2</sub> methanation on Ru/TiO<sub>2</sub> catalysts: unravelling the decisive role of the TiO<sub>2</sub> support crystal structure. *Catal. Sci. Technol.* **2016**, *6*, 8117-8128.
- (7) Lin, Q.; Liu, X. Y.; Jiang, Y.; Wang, Y.; Huang, Y.; Zhang, T. Crystal phase effects on the structure and performance of ruthenium nanoparticles for CO<sub>2</sub> hydrogenation. *Catal. Sci. Technol.* **2014**, *4*, 2058-2063.
- (8) Lamic, A. F.; Pham, T. L. H.; Potvin, C.; Manoli, J. M.; Mariadassou, G. D. Kinetics of bifunctional isomerization over carbides (Mo, W). *J. Mol. Catal. A-Chem.* **2005**, *237*, 109-114.
- (9) Ma, Y.; Guan, G.; Hao, X.; Zuo, Z.; Huang, W.; Phanthong, P.; Kusakabe, K.; Abudula, A. Highly-efficient steam reforming of methanol over copper modified molybdenum carbide. *RSC. Adv.* **2014**, *4*, 44175-44184.
- (10) Shi, C.; Zhang, A.; Li, X.; Zhang, S.; Zhu, A.; Ma, Y.; Au, C. Ni-modified Mo<sub>2</sub>C catalysts for methane dry reforming. *Appl. Catal. A: Gen.* **2012**, *431-432*, 164-170.
- (11) Christensen, J. M.; Duchstein, L. D. L.; Wagner, J. B.; Jensen, P. A.; Temel, B.; Jensen, A. D. Catalytic Conversion of Syngas into Higher Alcohols over Carbide Catalysts. *Ind. Eng. Chem. Res.* **2012**, *51*, 4161-4172.
- (12) Liu, C.; Lin, M.; Jiang, D.; Fang, K.; Sun, Y. Preparation of Promoted Molybdenum Carbides Nanowire for CO Hydrogenation. *Catal. Lett.* **2014**, *144*, 567-573.
- (13) Yin, K.; Shou, H.; Ferrari, D.; Jones, C. W.; Davis, R. J. Influence of Cobalt on Rubidium-Promoted Alumina-Supported Molybdenum Carbide Catalysts for Higher Alcohol Synthesis from Syngas. *Top. Catal.* **2013**, *56*, 1740-1751.

- (14) Xu, W.; Ramirez, P. J.; Stacchiola, D.; Rodriguez, J. A. Synthesis of  $\alpha$ -MoC<sub>1-x</sub> and  $\beta$ -MoC<sub>y</sub> Catalysts for CO<sub>2</sub> Hydrogenation by Thermal Carburization of Mo-oxide in Hydrocarbon and Hydrogen Mixtures. *Catal. Lett.* **2014**, *144*, 1418-1424.
- (15) Posada-Pérez, S.; Viñes, F.; Ramirez, P. J.; Vidal, A. B.; Rodriguez, J. A.; Illas, F. The bending machine: CO<sub>2</sub> activation and hydrogenation on  $\delta$ -MoC(001) and  $\beta$ -Mo<sub>2</sub>C(001) surfaces. *Phys. Chem. Chem. Phys.* **2014**, *16*, 14912-14921.
- (16) Rodriguez, J. A.; Evans, J.; Feria, L.; Vidal, A. B.; Liu, P.; Nakamura, K.; Illas, F. CO<sub>2</sub> hydrogenation on Au/TiC, Cu/TiC, and Ni/TiC catalysts: Production of CO, methanol, and methane. *J. Catal.* **2013**, *307*, 162-169.
- (17) Xu, W.; Ramirez, P. J.; Stacchiola, D.; Brito, J. L.; Rodriguez, J. A. The carburization of transition metal molybdates (M<sub>x</sub>MoO<sub>4</sub>, M=Cu, Ni or Co) and the generation of highly active metal/carbide catalysts for CO<sub>2</sub> hydrogenation. *Catal. Lett.* **2015**, *145*, 1365-1373.
- (18) Liu, X.; Song, Y.; Geng, W.; Li, H.; Xiao, L.; Wu, W. Cu-Mo<sub>2</sub>C/MCM-41: An Efficient Catalyst for the Selective Synthesis of Methanol from CO<sub>2</sub>. *Catalysts* **2016**, *6*, 75.
- (19) Nagai, M.; Oshikawa, K.; Kurakami, T.; Miyao, T.; Omi, S. Surface Properties of Carbided Molybdena-Alumina and Its Activity for CO<sub>2</sub> Hydrogenation. *J. Catal.* **1998**, *180*, 14-23.
- (20) Moreno-Castilla, C.; Salas-Peregrín, M. A.; López-Garzón, F. J. Hydrogenation of carbon oxides by Ru/activated carbon catalysts obtained from Ru<sub>3</sub>(CO)<sub>12</sub>: effect of pretreatment on their dispersion, composition and activity. *J. Mol. Catal. A: Chem.* **1995**, *95*, 223-233.
- (21) Jiménez-Villacorta, F.; Álvarez-Fraga, L.; Bartolomé, J.; Climent-Pascual, E.; Salas-Colera, E.; Aguilar-Pujol, M. X.; Ramírez-Jiménez, R.; Cremades, A.; Prieto, C.; Andrés, A. Nanocrystalline cubic ruthenium carbide formation in the synthesis of graphene on ruthenium ultrathin films. *J. Mater. Chem. C.* **2017**, *5*, 10260-10269.
- (22) Zhao, Z.; Meng, C.; Li, P.; Zhu, W.; Wang, Q.; Ma, Y.; Shen, G.; Bai, L.; He, H.; He, D.; Yu, D.; He, J.; Xu, B.; Tian, Y. Carbon coated face-centered cubic Ru-C nanoalloys. *Nanoscale* **2014**, *6*, 10370-10376.
- (23) Sun, W.; Chakraborty, S.; Ahuja, R. Stabilizing a hexagonal Ru<sub>2</sub>C via Lifshitz transition under pressure. *Appl. Phys. Lett.* **2013**, *103*, 251901.
- (24) Sanjay Kumar, N. R.; Chandra Shekar, N. V.; Chandra, S.; Basu, J.; Divakar, R.; Sahu, P. C. Synthesis of novel Ru<sub>2</sub>C under high pressure-high temperature conditions. *J. Phys.: Condens. Matter.* **2012**, *24*, 362202.
- (25) Abe, T.; Tanizawa, M.; Watanabe, K.; Taguchi, A. CO<sub>2</sub> methanation property of Ru nanoparticle-loaded TiO<sub>2</sub> prepared by a polygonal barrel-sputtering method. *Energy Environ. Sci.* **2009**, *2*, 315-321.

(26) Li, D.; Ichikuni, N.; Shimazu, S.; Uematsu, T. Hydrogenation of CO<sub>2</sub> over sprayed Ru/TiO<sub>2</sub> fine particles and strong metal-support interaction. *Appl. Catal. A: Gen.* **1990**, *180*, 227-235.

(27) Li, Y.; Zhang, L. A.; Qin, Y.; Chu, F.; Kong, Y.; Tao, Y.; Li, Y.; Bu, Y.; Ding, D.; Liu, M. Crystallinity Dependence of Ruthenium Nanocatalyst toward Hydrogen Evolution Reaction. *ACS Catal.* **2018**, *8*, 5714-5720.

(28) Martínez Tejada, L. M.; Muñoz, A.; Centeno, M. A.; Odriozola, J. A. In-situ Raman spectroscopy study of Ru/TiO<sub>2</sub> catalyst in the selective methanation of CO. *J. Raman Spectrosc.* **2016**, *47*, 189-197.

(29) Sadezky, A.; Muckenhuber, H.; Grothe, H.; Niessner, R.; Pöschl, U. Raman microspectroscopy of soot and related carbonaceous materials: Spectral analysis and structural information. *Carbon* **2005**, *43*, 1731-1742.

(30) Tougaard, S. QUASES: Software packages to characterize surface nano-structures by analysis of electron spectra. <http://www.quases.com/products/quases-imfp-tp2m/>

(31) Morgan, D. J. Resolving ruthenium: XPS studies of common ruthenium materials. *Surf. Interface Anal.* **2015**, *47*, 1072-1079.

(32) Teschner, D.; Borsodi, J.; Wootsch, A.; Révay, Z.; Hävecker, M.; Knop-Gericke, A.; Jackson S. D., Schlögl, R. The Roles of Subsurface Carbon and Hydrogen in Palladium-Catalyzed Alkyne Hydrogenation. *Science* **2008**, *320*, 86-89.

(33) Park, J.; Lee, J. W.; Ye, B. U.; Chun, S. H.; Joo, S. H.; Park, H.; Lee, H.; Jeong, H. Y.; Kim, M. H.; Baik, J. M. Structural Evolution of Chemically-Driven RuO<sub>2</sub> Nanowires and 3-Dimensional Design for Photo-Catalytic Applications. *Scientific Reports* **2015**, *5*, 11933.

(34) Liu, J.; Zhang, L. L.; Zhang, J.; Liu, T.; Zhao, X. S. Bimetallic ruthenium-copper nanoparticles embedded in mesoporous carbon as an effective hydrogenation catalyst *Nanoscale* **2013**, *5*, 11044-11050.

(35) Wang, X.; Hong, Y.; Shi, H.; Szanyi, J. Kinetic modeling and transient DRIFTS-MS studies of CO<sub>2</sub> methanation over Ru/Al<sub>2</sub>O<sub>3</sub> catalysts. *J. Catal.* **2016**, *343*, 185-195.

(36) Hertrich, M. F.; Scharnagl, F. K.; Pews-Davtyan, A.; Kreyenschulte, C. R.; Lund, H.; Bartling, S.; Jackstell, R.; Beller, M. Supported Cobalt Nanoparticles for Hydroformylation Reactions. *Chem. Eur. J.* **2019**, *25*, 5534-5538.

(37) Marwood, M.; Doepper, R.; Renken, A. In-situ surface and gas phase analysis for kinetic studies under transient conditions: The catalytic hydrogenation of CO<sub>2</sub>. *Appl. Catal. A: Gen.* **1997**, *151*, 223-246.

(38) Panagiotopoulou, P.; Kondarides, D. I.; Verykios, X. E. Mechanistic aspects of the selective methanation of CO over Ru/TiO<sub>2</sub> catalyst. *Catal. Today* **2012**, *181*, 138-147.

(39) Sachtler, J. W. A.; Kool, J. M.; Ponec, V. The role of carbon in methanation by cobalt and ruthenium. *J. Catal.* **1979**, *56*, 284-286.

(40) Panagiotopoulou, P.; Verykios, X. E. Mechanistic Study of the Selective Methanation of CO over Ru/TiO<sub>2</sub> Catalysts: Effect of Metal Crystallite Size on the Nature of Active Surface Species and Reaction Pathways. *J. Phys. Chem. C* **2017**, *121*, 5058-5068.

(41) Zhao, K.; Wang, L.; Calizzi, M.; Moioli, E.; Züttel, A. In Situ Control of the Adsorption Species in CO<sub>2</sub> Hydrogenation: Determination of Intermediates and Byproducts. *J. Phys. Chem. C* **2018**, *122*, 20888-20893.

(42) Eckle, S.; Anfang, H. G.; Behm R. J.; Reaction Intermediates and Side Products in the Methanation of CO and CO<sub>2</sub> over Supported Ru Catalysts in H<sub>2</sub>-Rich Reformate Gases. *J. Phys. Chem. C* **2011**, *115*, 1361-1367.

▪ GRAPHICAL ABSTRACT (“For Table of Contents Only”)

